IEEE Access
Multidisciplinary | Rapid Review | Open Access Journal

Received November 8, 2019, accepted November 15, 2019, date of publication November 20, 2019, date of current version December 4, 2019.

Digital Object Identifier 10.1109/ACCESS.2019.2954489

Optimization of Postural Transition Scheme for Quadruped Robots Trotting on Various Surfaces

JEONG HOON LEE AND JONG HYEON PARK, (Member, IEEE)
Department of Mechanical Engineering, Hanyang University, Seoul 133-791, South Korea
Corresponding author: Jong Hyeon Park (jongpark@hanyang.ac.kr)

ABSTRACT Achieving stable trotting of quadruped robots on various surfaces is challenging because they lose balance due to the displacement of their center of gravity (COG) and undesirable impulse forces. This paper proposes schemes for postural transition and robust posture control, thus enabling quadruped robots to trot on horizontal and slanted surfaces. For a region connected by surfaces with different angles, the postural transition scheme (PTS) is implemented by the movement values optimized by a real-coded genetic algorithm (RCGA), which regulates the location of the center of gravity (COG) projection point of robots. In addition, the movement values are applied to the center points of the desired foot trajectories by using cubic polynomial, which is able to generate adaptive foot motion continuously and gradually. For robust posture control, admittance control with impedance modulation (IM) is applied to the foot trajectories, which changes the impedance parameters in real-time depending on the magnitude of the disturbances, such as the excessive swaying of the robot body that cause instabilities in the robot posture during locomotion. Control thresholds regulated by the angular speed of the robot body are proposed as a criterion for controlling the excessive swaying by IM. Computer simulations and hardware experiments were carried out to verify the performance of the proposed schemes.

INDEX TERMS Quadruped robots, slope, admittance control, impedance modulation, posture control, stable locomotion, genetic algorithm, optimization.

I. INTRODUCTION

In general, legged robots have an advantage over other terrestrial mobile robots in that they can equally move in sandy, rough, rocky, and steep terrains. Among many legged robots, quadrupeds offer a viable solution exhibiting locomotion stability and velocity at the same time [1]–[7]. The locomotion of quadruped robots is generally categorized into five types depending on the leg positions and gait speeds: walking, trotting, cantering, bounding and galloping (with transverse or rotary patterns). The trotting motion, which is the main topic in this paper, is a locomotion of middle-range speed, where a diagonally positioned pair of legs support the body whereas the other pair is simultaneously lifted from the ground and prepares the landing for the next step. Trotting is more energy-efficient locomotion for quadrupeds than any other types of locomotion. Therefore, trotting has attracted significant interest in the research on locomotion of quadruped robots [8]–[11]. Trajectory generation of legged robots can be classified depending on whether it is based on modeling or not. In a model-based method, such as the linear inverted pendulum (LIPM) [12] and gravity-compensated inverted pendulum models (GCIPM) [13], each robot is modeled as a single or a few point masses. On the other hand, in a model-free method, a trajectory of a legged robot is generated without any dynamic model. Model-free methods include central pattern generators (CPGs) [14]–[16] and the ellipsoidal foot trajectory [17]. In the former, a rhythmic motion pattern of each active joint is generated by a simple artificial neural network and in the latter, a cyclic and smooth motion for each foot is designed to yield a path on an ellipsoid. Since any trajectory generated by a model-free method does not guarantee stable locomotion, however, characteristic hardware designs of robot legs or control schemes to ensure locomotion stability are needed. For locomotion stability, the feet of the robots should be able to adapt appropriately to the uncertain ground profile. For stable foot landing, along with the use of back-drivable actuators and/or force sensors, various control methods such as fuzzy control, adaptive control, force control, and impedance control have been

The associate editor coordinating the review of this manuscript and approving it for publication was Aysegul Ucar.

extensively proposed [16], [18]–[24]. Particularly, it has been shown that impedance control helps to maintain robot posture balance by regulating the impulsive ground-reaction force and adapting to uncertainty on the ground profile and that the use of variable impedance or impedance modulation (IM) is effective [25]–[27].

Locomotion stability is mainly evaluated by a static or a dynamic stability margins [28]. The former is based on a support polygon and the projection of the center of gravity (COG), under the assumption of quasi-static motions [14], [29]. On the other hand, the latter takes forces/moments generated during locomotion as well as the speed and acceleration of the robot into consideration, mainly based on the zero-moment point (ZMP) or the center of pressure (COP) [30]. In trotting, the support polygon does not exist and is rather collapsed into a line segment; therefore, it is not appropriate to use a static stability margin to evaluate the trotting stability [31].

As the main contribution, this paper proposes the followings in order to increase the stability of trotting quadrupeds, further improving the authors' previous work [18].

1) The quadrupeds perform the postural transition scheme (PTS) to trot sequentially on surfaces with different angles, which regulates the COG projection of the robot.
2) The proposed PTS is optimized by using a real-coded genetic algorithm (RCGA) [32]–[34] based on the reproduction operator of gradient-like selection [35]. This further improves the stability of quadrupeds, particularly in moving through regions where slopes in the trail change.
3) Control thresholds regulated by the angular speeds of the robot body are proposed as a criterion of the swaying for performing the IM.
4) Admittance control with the IM is proposed and implemented, which changes the impedance parameters in real-time based on ranges generated by the control thresholds.

The rest of this paper is organized as follows: In Section II, the generation of the ellipsoidal foot trajectories for trotting, an introduction to the PTS, the proposed admittance control with the IM, and the definitions of the control thresholds are described. Section III describes the computer simulations and experiments with a quadruped robot named HUNTER (Hanyang UNiversity TEtrapod Robot) developed at the authors' lab to verify the effectiveness of the proposed schemes. Section IV concludes this work with a summary.

II. GENERATION OF FOOT TRAJECTORIES AND THE POSTURE CONTROL SCHEME

When a quadruped animal meets a hill while walking on a trail, it changes its body posture, for example, by lowering its head, bending its front legs down, stretching its rear legs back, or moving its torso forward. These behavioral patterns become more clearly observable as the trail becomes steeper.

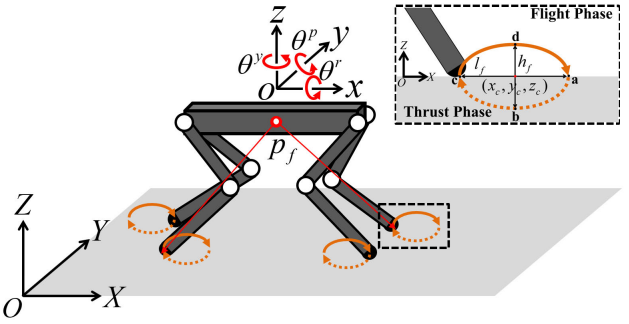

FIGURE 1. Coordinate frames and the model of a quadruped robot. The solid and dotted lines shown indicate a flight phase and a thrust phase, respectively.

Here, schemes that mimic the behaviors of animals are proposed for quadruped robots in order to make them trot stably in a diverse trail.

A. ELLIPSOIDAL FOOT TRAJECTORY

Here, for a trotting quadruped, the trajectory for each foot is generated based on an ellipsoid. The ellipsoidal foot trajectory has the advantage of being continuous and rhythmical. In addition, it is intuitive and easy to analyze. However, its parameter should be changed for adoption to the changing environment of the trail.

First, let's define a fixed global and a body-attached coordinate frames, which are shown in Fig. 1, where coordinate frames $\{XYZ\}$ and $\{xyz\}$ denote the fixed and the body coordinate frames, respectively. The Z-axis of the global coordinate frame is defined to be vertically upward, i.e., perfectly opposite to the direction of the gravitational field. Let θ^r, θ^p, and θ^y denote the Euler angles of the body in the roll, pitch, and yaw-directions. Let h_f and l_f denote the parameters of an ellipsoidal foot trajectory, i.e., the stride and the vertical range of the foot action, respectively. The stride in the first step is set as a half of that in the normal trot cycles under the assumption that the quadruped is stationary before start trotting. Without loss of generality, it is assumed that the quadruped robot moves in the X-direction unless stated otherwise.

The ellipsoidal foot trajectory consists of a flight phase and a thrust (or stance) phase. Let $\mathbf{x}_f^{ij} \triangleq [x_f^{ij}\ y_f^{ij}\ z_f^{ij}]^T$ denotes the desired foot position of foot ij, where $i \in \{\text{Left, Right}\}$ and $j \in \{\text{Front, Rear}\}$, w.r.t. (with respect to) the body coordinate frame $\{xyz\}$:

$$x_f^{ij}(t) = l_f/2 \cdot \sin\left(\omega_f t + \phi\right) + x_c^{ij}(t), \tag{1}$$

$$y_f^{ij}(t) = y_c^{ij}(t), \tag{2}$$

$$z_f^{ij}(t) = h_f/2 \cdot \cos\left(\omega_f t + \phi\right) + z_c^{ij}(t), \tag{3}$$

where $0 \le t \le T$; l_f denotes the stride and h_f denotes the vertical motion range of the foot, which can be changed at the beginning of each step; angle ϕ is the initial phase which is set at $\pi/2$ for the pair of legs starting a thrust phase first and at $-\pi/2$ for the pair of legs starting a flight phase first; T denotes the step period and $\omega_f = 2\pi/T$ is the step frequency;

$\mathbf{x}_c^{ij} \triangleq [x_c^{ij}(t)\ y_c^{ij}(t)\ z_c^{ij}(t)]^T$ denotes the relative position of the center of the elliptic path for foot ij w.r.t. the body coordinate frame. Note that the distance between the center of the elliptic path of a foot and its associated shoulder (or the hip) is bounded from above by the length of the leg.

In this paper, the height of the thrust phase is set to zero in order to minimize the swaying of the robot body. Thus, the shape of the desired foot trajectory becomes a half ellipsoid. In addition, the orientation of the ellipsoidal path of a foot can be modified based on the slope of the trail and the orientation of the robot body. In order to secure a ellipsoidal path symmetric about the trail line and to reflect the trail slope, the desired position of the foot, $\mathbf{x}_f^d$, relative to the body frame is set as

$$\mathbf{x}_f^d = \mathbf{R}(\psi_t)\,(\mathbf{x}_f - \mathbf{x}_c) + \mathbf{x}_c, \tag{4}$$

where $\mathbf{R}(\psi_t)$ denotes the rotation matrix defined by

$$\mathbf{R}(\psi_t) = \begin{bmatrix} \cos\psi_t & 0 & -\sin\psi_t \\ 0 & 0 & 0 \\ \sin\psi_t & 0 & \cos\psi_t \end{bmatrix},$$

where ψ_t denotes the difference between the slope of the trail in the pitch-direction, γ, and the pitch angle of the robot body, θ^p, i.e.,

$$\psi_t \triangleq -\gamma + \theta^p. \tag{5}$$

Note that since the moving direction is assumed to be in the X-direction of the global coordinate frame, $\gamma < 0$ for an uphill trail.

B. POSTURAL TRANSITION SCHEME (PTS) AT POSTURE TRANSITION REGION

Under the assumption that the speed of quadruped's trotting is not high, quasi-static stability analysis is used here. First, suppose the quadruped robot meets a hill during trotting. If it maintains its posture used in a trot on a horizontal flat track, its COG projection point (in static locomotion) on the ground would shift backward, thus making locomotion less stable in the sense of static stability margin [28]. Thus, to prevent this from happening, its posture needs to be changed depending on the slope of the trail.

After detecting a hill, the quadruped needs to change its posture according to some schemes, which are called in general postural transition schemes (PTS). Some examples of the PTS are shown in Fig. 2, where the legs of the simplified robot model are virtual without any knee or elbow joints. One scheme is to shift the body forward, thus the COG projection of the robot does not move backward so that it is located somewhere in the middle of front legs and rear legs (see Fig. 2(a)). Another is to lower the level of its shoulder so that it is closer to the ground and the longitudinal direction of the robot body is aligned almost parallel (Fig. 2(b)) or somewhat oblique (Fig. 2(c)) to a horizontal line. This scheme, combined with the previous, achieves secure footing on the ground and enhances the stability by lowering the COG further. Since there may be many different varieties of the PTS,

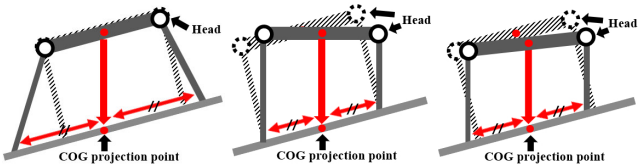

FIGURE 2. Some examples of postural transition schemes for an uphill trail: (a) moving the legs forward and backward, (b) lowering the front legs and maintaining almost horizontal body posture (c) lowering the front legs and maintaining a some acute angle between the body and the horizontal line.

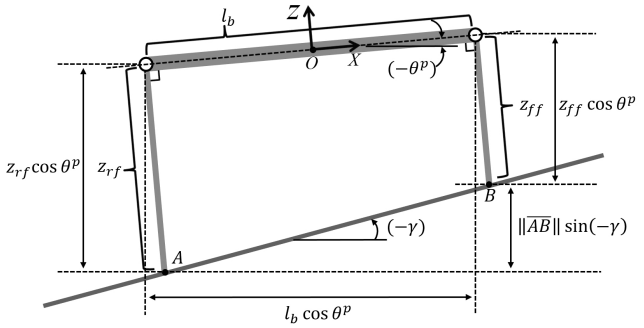

FIGURE 3. Geometrical shape of the robot with the front legs and the rear legs moving in the vertical direction for an uphill trail.

in this work, the optimization of the PTS is proposed based on the RCGA. The optimized movements of the legs are demonstrated in the simulations covered in Section III.

Note that there exists a geometrical constraint

$$\frac{z_{ff} - z_{rf}}{\ell_b}\cos\theta^p + \sin\theta^p = \frac{\sin\gamma}{\cos(\theta^p - \gamma)}, \tag{6}$$

where ℓ_b is the longitudinal length of the robot, z_{ff} and z_{rf} respectively denote the z-coordinate of the body coordinate frame for the front and rear foot on the ground simultaneously. Thus, with this and (5),

$$\psi_t = \psi_t(\theta^p, z_{ff}, z_{rf}), \tag{7}$$

meaning that it is possible to the amount of angular adjustment of desired foot path by measuring body pitch angle and a set of the positions of front and rear feet in contact with the ground.

Moreover, the center of an elliptic foot path needs to be changed depending on the slope of the track. Thus, when the slope changes, the center position also needs to be changed. So, the center position is a function of the track slop. The optimal position of the center of an elliptic path will be determined based on the genetic algorithm, which will be explained later. If there is a change in the slope of the track while totting in the track, region k, the center of an elliptic foot path needs to be gradually changed to the optimal value of the subsequent slope of the track, called region $(k+1)$. Let's assume that this transition takes N steps of trot. Here, a cubic polynomial is used to deal with the gradual change in $\mathbf{x}_c^{ij}$ for foot ij. The transitional position of the center of

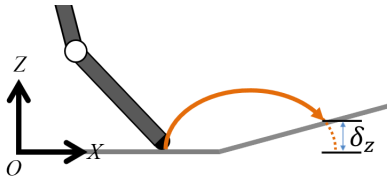

FIGURE 4. Premature ground contact for postural transition: δ_z occurs by premature ground contact between the foot and the slanted surface by the desired foot trajectory at the region meeting the surfaces with different angles.

the elliptic path for foot ij at the transition step number n $(1 \le n \le N)$ becomes

$$\mathbf{x}_c^{ij(n)}(t) = \mathbf{x}_{c,k}^{ij} + \sum_{q=0}^{3} \boldsymbol{\xi}_q^{ij} t^q, \quad 0 < t \le T, \tag{8}$$

with conditions

$$\begin{aligned} \mathbf{x}_c^{ij(n)}(0) &= \mathbf{x}_{c,k}^{ij} + (\mathbf{x}_{c,k+1}^{ij} - \mathbf{x}_{c,k}^{ij})\frac{n-1}{N}, \\ \dot{\mathbf{x}}_c^{ij(n)}(0) &= \dot{\mathbf{x}}_c^{ij(n)}(T) = \mathbf{0}, \\ \mathbf{x}_c^{ij(n)}(T) &= \mathbf{x}_{c,k}^{ij} + (\mathbf{x}_{c,k+1}^{ij} - \mathbf{x}_{c,k}^{ij})\frac{n}{N}. \end{aligned}$$

C. ADMITTANCE CONTROL WITH IMPEDANCE MODULATION (IM) REGULATED BY CONTROL THRESHOLD

Even with the PTS implemented, a control law should be implemented in order to deal with uncertainty in the geometry of the track. An unexpected change in the track slope may result in a premature ground contact of the landing feet, one of the example situations is described in Fig. 4. The admittance control, or impedance control in a large sense, is highly effective in controlling premature ground contact, which allow vertical positional adjustment, δ_z of the landing foot based on the ground reaction force in the vertical direction, f_z. This is summarized in the block diagram shown in Fig. 5.

Besides, in order to enhance further the stability of trotting with slope changes, modulating the impedance parameters for the admittance control is proposed. The impedance parameters are gradually based on where the foot position is on its elliptic path. In this paper, the main task of admittance control maintains the posture balance of the robot by controlling the stiffness of the legs. Admittance control in the forward and lateral direction is not considered in this work because of the limitations of the force sensitive resistors (FSR) used in hardware experiments that can only measure the magnitude of the force.

For a flexible implementation of the admittance control with impedance modulation, let's assume that N_z sets of impedance parameters are used for a single step motion for each foot and that each set is used for an equal duration of time, T/N_z. The equations defining the admittance control with the impedance modulation can be written as a 2nd-order differential vector equation. For $i \in \{1, 2, \ldots, N_z\}$,

$$M_i(\boldsymbol{\theta})\ddot{\delta}_z + B_i(\boldsymbol{\theta})\dot{\delta}_z + K_i(\boldsymbol{\theta})\delta_z = f_z \tag{9a}$$

or

$$\ddot{\delta}_z = \frac{1}{\mathbf{M}_i(\boldsymbol{\theta})}(f_z - B_i(\boldsymbol{\theta})\dot{\delta}_z - K_i(\boldsymbol{\theta})\delta_z), \tag{9b}$$

where

$$\begin{aligned} M_i(\boldsymbol{\theta}) &= (\sigma_i - \varepsilon_i\|\boldsymbol{\theta}\|)/\zeta_i, \\ B_i(\boldsymbol{\theta}) &= 2\sqrt{M_i(\boldsymbol{\theta})K_i}, \\ K_i &= (K_0 + \mu_i K_v^{\pi})/\zeta_i, \\ \delta_z &= z_f - z_f^d, \quad \boldsymbol{\theta} = \begin{bmatrix}\theta^r & \theta^p\end{bmatrix}^T; \end{aligned}$$

ε_i, μ_i, σ_i and ζ_i are constants; z_f and z_f^d denote the measured and the desired vertical positions of each foot, respectively; f_z denotes the vertical ground reaction force (GRF); and K_0 and K_v^{π} are stiffness-related constants, where $\pi \in \{r, p\}$, where superscripts 'r' and 'p' standing for roll and pitch, respectively. K_0 and K_v^{π} use the values optimized by the RCGA. The offset position, δ_z, to be added to the desired foot trajectory in the diagram shown in Fig. 5 is computed by integrating $\ddot{\delta}_z$ over time twice. Parameter ε_i is zero when M_i is used as the desired mass with a fixed value, whereas ε_i is larger than one when M_i is used as the desired mass with values changed depending on the swaying of the robot body. Parameter μ_i is zero when the magnitude of sway in the pitch and roll-directions is small. Otherwise, depending on the magnitude of the sway, μ_i is changed, resulting in

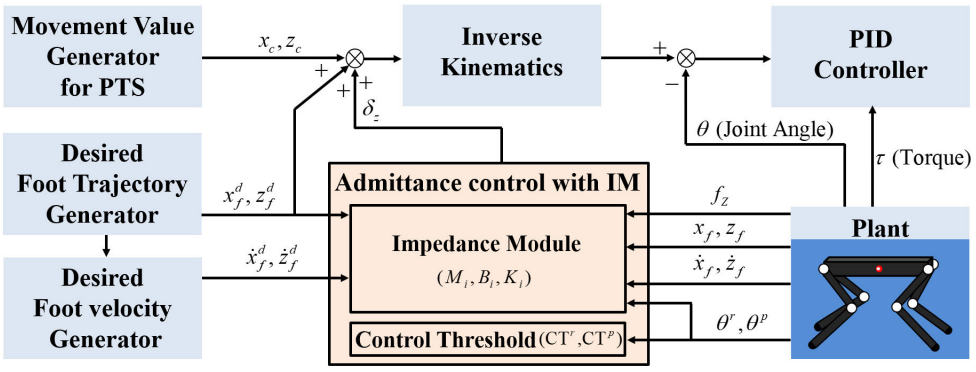

FIGURE 5. Block diagram of foot motion generator with admittance control with the IM.

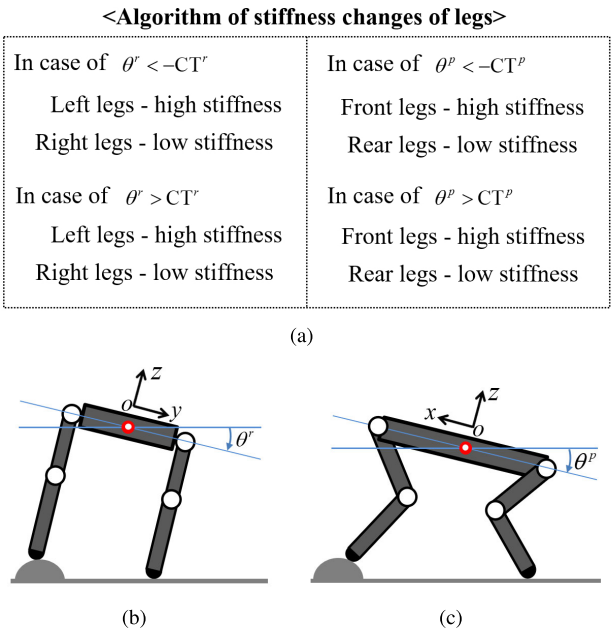

FIGURE 6. Impedance modulation: (a) Algorithm of stiffness changes of legs depending on the body angles, (b) An example of the algorithm of stiffness change for the roll angle: For admittance control, if $\theta^r < -\mathrm{CT}^r$, left legs need high stiffness whereas right legs need low stiffness, (c) An example of the algorithm of stiffness change for the pitch angle: For admittance control, if $\theta^p > \mathrm{CT}^p$, front legs need low stiffness, whereas rear legs need high stiffness.

impedance modulation. More specifically, each of the roll angle and the pitch angle are categorized into $N_s + 1$ level depending on its size. If $|\theta^r| \in \mathrm{SR}_k^r$ and $|\theta^p| \in \mathrm{SR}_q^p$, where $\mathrm{SR}_k^\pi = [\mathrm{SR}_0^\pi + \eta_{k-1}^\pi, \mathrm{SR}_0^\pi + \eta_k^\pi]$ with $k, q \in \{1, 2, \ldots, N_s\}$ for $\pi = r, p$,

$$\mu_i = \pm\alpha_k^r \pm \alpha_q^p,$$

where α^π with the positive sign is used when high stiffness is required, whereas one with the negative sign is used when low stiffness is required. The robot determines whether to use high stiffness or low stiffness depending on the magnitude and the direction of the body angles, as can be seen in Fig. 6. Note that the set of η^π's denotes the level of the sway of the robot body, $\eta_{k-1}^\pi = (k-1)\nu^\pi$ and $\eta_{N_s}^\pi = \infty$, where ν^π denotes a contant and $\alpha_0^\pi = 0$ under the condition

$$\alpha_i^\pi \le \alpha_{i+1}^\pi, \quad i = 1, \ldots, N_s - 1,$$

for $\pi = r, p$. In this work, N_s is set to 6 and α^π and ν^π use the values optimized by the RCGA. SR_0^π is defined by

$$\mathrm{CT}^r \triangleq \mathrm{SR}_0^r = |\beta^r - P_i^r|,$$
$$\mathrm{CT}^p \triangleq \mathrm{SR}_0^p = |\beta^p - P_i^p| + \mathbf{f}_{\psi_t}(t),$$

where the CT^π denotes the control threshold regulated by the angular speeds of the robot body. β^π denotes the initial value of SR_0^π, whose value is optimized by the RCGA. P_m^π with $m \in \{1, 2, \ldots, N_z\}$ for $\pi = r, p$ is defined as

$$P_m^\pi = \kappa^\pi \left(\frac{\theta^\pi - \theta_m^\pi}{T/N_z} \right),$$

where κ^π is coefficients to regulate the scales of P_m^π not to exceed β^π. The trotting is a gait of middle speed with dynamic properties, although it is considered as quasi-static one in this paper. For reflecting the dynamic properties, thus, the CT^π is regulated by P_m^π in which the angular speeds of the robot body is expressed as the coefficients. A cubic polynomial is used to deal with the gradual change in $\mathbf{f}_{\psi_t}$ for SR_0^p, which reflects the pitch angle of the robot body and the slope of the trail changed by the PTS. The transitional angle $\mathbf{f}_{\psi_t}{}^{(n)}$ at the transition step number n ($1 \le n \le N$) and the regions k and $(k+1)$ as in (8) becomes

$$\mathbf{f}_{\psi_t}{}^{(n)}(t) = \psi_{t,k} + \sum_{q=0}^{3} \epsilon_q t^q, \quad 0 < t \le T, \tag{10}$$

with conditions

$$\mathbf{f}_{\psi_t}{}^{(n)}(0) = \psi_{t,k} + (\psi_{t,k+1} - \psi_{t,k})\frac{n-1}{N},$$
$$\dot{\mathbf{f}}_{\psi_t}{}^{(n)}(0) = \dot{\mathbf{f}}_{\psi_t}{}^{(n)}(T) = \mathbf{0},$$
$$\mathbf{f}_{\psi_t}{}^{(n)}(T) = \psi_{t,k} + (\psi_{t,k+1} - \psi_{t,k})\frac{n}{N}.$$

It is well known that if an excessive transient behavior of the vertical GRF of the landing foot is one of the key factors that destabilize the robot posture. In addition, the moment of the maximum height of the flight phase is an important factor destabilizing the robot posture. The foot located at the maximum height during the flight phase can be contacted on the ground by rotating the robot body with respect to the support line. Assuming that the two legs in the diagonal position generating the support line do not fall off the ground, the swaying of the robot body generated by the rotation are largest in size. Thus, in this paper, it is suggested that $N_z = 2$ or 4.

In fact, the swaying is not present during ideal trotting motion because the robot trots with constant strides and foot heights. However, if the swaying always exists, we will call them non-specific swaying, which occurs due to a combination of the following several factors:

- Inertia force caused by dynamic gait
- Foot bouncing caused by ground contact
- Thrust phase of the ellipsoidal foot trajectory
- Tracking errors changing the desired foot trajectory
- Differences in the mechanical structure of the front leg and rear leg

Thus, the ranges generated by CT^r and CT^p can be explained as the angle ranges of the robot body allowing non-specific swaying while regulating swaying beyond the non-specific ones. Thus, in this work, the stable control of robot posture eventually means the roll and pitch angles (the swaying) are kept within the ranges generated by CT^r and CT^p, and the control methods are the optimized PTS and admittance control with the IM.

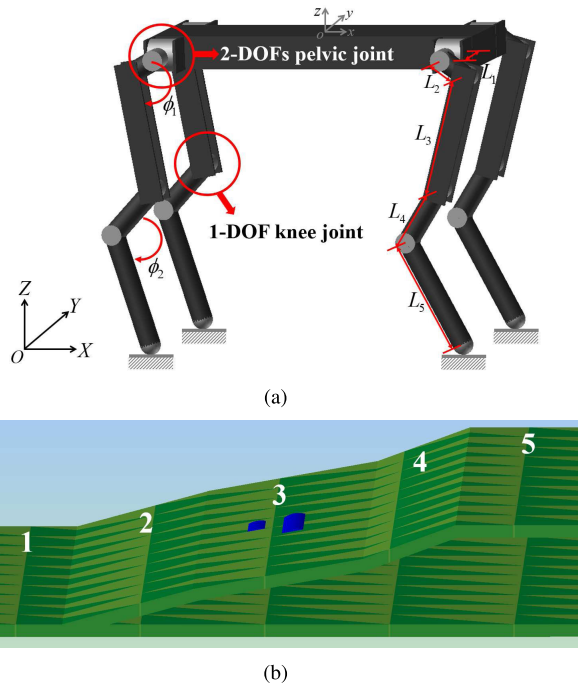

FIGURE 7. Simulation model: (a) Quadruped robot, (b) Horizontal, slanted, and irregular terrain models: In the order that the robot trots forward, 1. Horizontal surface, 2. Slanted surface with 1.1 m and 15 degrees, 3. Irregular surface with the heights of 0.015 m and 0.020 m from the left one and slanted surface with 1.4 m and 10 degrees, 4. Slanted surface with 0.8 m and 20 degrees, 5. Horizontal surface.

TABLE 1. Parameters of the quadruped robot.

Part	Value	Part	Value
Length†	0.508 (m)	Link3 (L3)	0.200 (m)
Width†	0.196 (m)	Link4 (L4)	0.105 (m)
Height†	0.050 (m)	Link5 (L5)	0.197 (m)
Weight	24.462 (kg_f)	ϕ_1	1.920 (rad)
Link1 (L1)	0.056 (m)	ϕ_2	2.096 (rad)
Link2 (L2)	0.050 (m)	-	-

† Robot body.

⊙ The simulation and hardware robot models possess the same specifications.

III. COMPUTER SIMULATIONS AND HARDWARE EXPERIMENTS

Computer simulations were performed to verify the effectiveness of the proposed schemes (the PTS and admittance control with the IM). In addition, the proposed schemes were implemented in a hardware model called HUNTER.

A. PARAMETER SETTINGS FOR THE SIMULATIONS

The robot model shown in Fig. 7(a) is a simplified hardware model (HUNTER), with its specifications listed in Table 1. HUNTER has four legs and each leg consists of a 2-DOF pelvic joint and a 1-DOF knee joint. The uphill trails consist of various tilt angles (10, 15, and 20 degrees), lengths (1.1, 1.4, and 0.8 m), and irregularities (heights of 0.015 and 0.020 m). For the irregular surface with the height of 0.015 m, the length for Y-direction is short when compared with that with the height of 0.020 m. The materials of the feet and the ground were assumed to be rubber and wood, respectively.

TABLE 2. Parameters of the model environment.

Symbol	Value	Unit	Symbol	Value	Unit
k	2,000	kN/m	m_3	2	-
c	1	kNs/m	μ_s	0.9	-
m_1	1.3	-	μ_d	0.6	-
m_2	1	-			

The simulation was conducted using Mathworks' Matlab software and a commercial dynamics simulator, RecurDyn. A contact model between the feet and the surface is very important for a realistic simulation. In this paper, the Hunt–Crossley model [36] is used as the contact model between the feet and the surface, where the normal component of the contact force is computed by

$$f_n = k\delta^{m_1} + c\frac{\dot{\delta}}{|\dot{\delta}|}|\dot{\delta}|^{m_2}\delta^{m_3}, \tag{11}$$

where k is the spring coefficient, c is the damping coefficient, and δ is a penetration value at the contact point between the foot and the surface. m_1, m_2, and m_3 are the exponents of the stiffness, damping, and indentation, respectively [37].

The values of k, c, m_1, m_2, and m_3 used for the simulations are summarized in Table 2. Based on the assumptions about the feet and ground materials, the values of the static friction coefficient μ_s and dynamic friction coefficient μ_d are also listed in Table 2.

B. COMPUTER SIMULATION I: OPTIMIZATION OF THE PTS

As introduced in Section II-B, the number of the PTS that satisfy the SSM is infinite. Thus, the RCGA is used to find the optimal PTS to achieve the most stable locomotion for the uphill trails.

The RCGA discussed in this paper includes a gradient-like reproduction operator and an elitist strategy, as can be seen in Fig. 8. In addition, Fig. 8 shows how the individuals are applied to the robot motion. The crossover probability, mutation probability, generation, and population size (meaning the design parameters of the RCGA) were set to 0.8, 0.2, 100, and 20, respectively. The design variables were the transitional position of (8) at $n = N$ and $t = T$. Let $x_c^{ij(N)}(T) \triangleq b_x^f$ (j = Front) or b_x^r (j = Rear) and $z_c^{ij(N)}(T) \triangleq b_z^f$ (j = Front) or b_z^r (j = Rear), where the transitional positions of the left legs and the right legs are equal. Their lower and upper boundary conditions considering the workspaces and kinematic singularities of the legs become

$$\begin{aligned} -0.160 \le b_x^f, \quad b_x^r \le 0.160, \\ -0.020 \le b_z^f, \quad b_z^r \le 0.150. \end{aligned}$$

Thus, the robot performed the PTS by moving the front legs and rear legs in the horizontal and vertical directions by

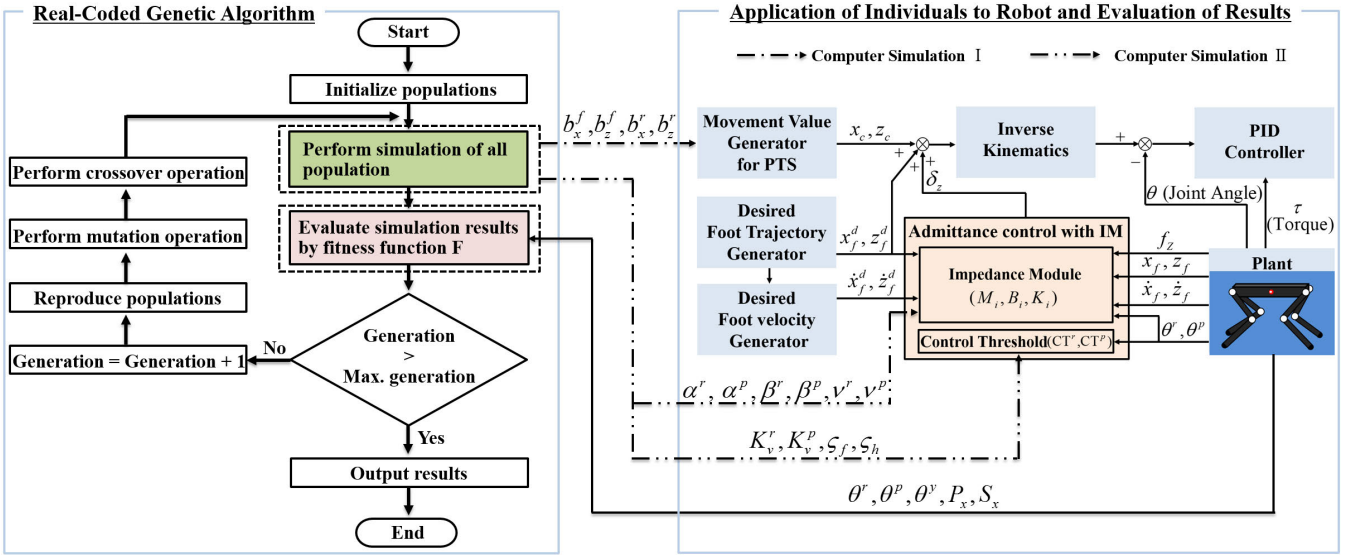

FIGURE 8. Flow chart of the RCGA and application to robot.

using the values of the optimized design variables. For the foot trajectory, the stride l_f was 0.080 m and the maximum foot height h_f was 0.100 m. The period T for a single step, composed of a flight phase and a thrust phase, was set to one second and total simulation time was 7.25 s. ψ_t was computed by (7). In this simulation, there were no posture control methods (including admittance control) used to verify the effectiveness of the isolated PTS. The simulations were performed by using the slanted surfaces with the angles from 7.5 to 20 degrees at intervals of 2.5 degrees.

The performance and stability of the robot locomotion was evaluated by the following fitness function:

$$F = \upsilon(f_a + f_p + f_s), \tag{12}$$

where

$$f_a = \frac{1}{1 + A_E} \times 100,$$
$$f_p = w_4 \frac{P_x}{P_d} \times 100,$$
$$f_s = \frac{1}{1 + w_5 |\min(S_x)|} \times 100, \quad \text{for } S_x < 0$$

where

$$A_E = w_1 \max(|\theta^r|) + w_2 \max(|\theta^p|) + w_3 \max(|\theta^y|),$$

where superscripts 'r', 'p' and 'y' standing for roll, pitch, and yaw respectively. The penalty coefficient is defined as

$$\upsilon = \begin{cases} 0, & \text{if } |\boldsymbol{\theta}| > 1 \\ 1, & \text{if } |\boldsymbol{\theta}| \leq 1 \end{cases}$$

where $\boldsymbol{\theta} = \left[\theta^r \ \theta^p \ \theta^y\right]^T$. υ is necessary to give penalty for large swaying that can cause tipping over, which becomes zero if $\boldsymbol{\theta}$ is above one radian. P_x is the forward displacement of the robot body during the locomotion, whose desired value $P_d = 2l_f N_t$, where N_t denotes the total number of the foot steps. S_x is the forward velocity of the robot body during the locomotion. Thus, f_a evaluates the sway of the robot body during the locomotion because the stability of the robot posture decreases as the swaying increases. f_p evaluates the performance of the forward movement of the robot and f_s evaluates backward foot slipping. w_1, w_2, w_3, w_4, and w_5 are the weights determining the importance of the variables of the scoring functions, whose values were set to 3, 1, 3, 2, and 0.1, respectively. In this paper, the control method of the robot posture in the yaw-direction is not included. However, the robot could trot without a large change of the yaw angle for the uphill trails because the robot locomotion was evaluated by f_a and f_p.

TABLE 3. Optimization results of individuals.

Slope angle	Best score	Design variable (m)			
		b_x^f	b_z^f	b_x^r	b_z^r
7.5°	338.85	−0.125	0.025	−0.051	−0.002
10.0°	311.11	−0.122	0.042	−0.056	−0.006
12.5°	296.95	−0.140	0.048	−0.073	−0.003
15.0°	278.31	−0.144	0.055	−0.074	−0.006
17.5°	259.08	−0.150	0.066	−0.068	−0.008
20.0°	242.09	−0.158	0.089	−0.053	−0.009

The aspects of the optimized PTS depending on the slope angle are summarized in Table 3. It is well known that the number of design variables greatly affects the simulation time. For reducing the simulation time, thus, the optimized values were used in the next subsection that the robot trots on the terrains with various slope angles. The postural transition performed by the optimized values exhibited unified shapes in which the legs moved together in the horizontal and

TABLE 4. Parameters set.

Region	Content	Simulation time	T. S. N†
I	Horizontal and slanted surface with 15 degrees	0∼13.25	4
II	The previous surface and slanted and irregular surface with 10 degrees	13.25∼28.25	2
III	The previous surface and slanted surface with 20 degrees	28.25∼39.25	2
IV	The previous surface and horizontal surface	39.25∼48.25	6

† T.S.N denotes the transition step number.

⊙ Each region includes the postural transition section meeting the surface of previous section.

vertical directions, as can be seen in Fig. 2(c). The resulting shapes have the advantage of reduced swaying and torque–in particular for knee joints–by distributing the movement of the legs in the horizontal and vertical direction. The robot bent its front legs to a greater degree in the vertical direction and stretched its front legs and rear legs to a greater degree in the horizontal direction according to the increasing slope angle. The score representing the performance and stability of the robot locomotion decreased with the increasing slope angle.

C. COMPUTER SIMULATION II: OPTIMIZATION OF THE TROTTING FOR TERRAIN WITH VARIOUS SLANTED SURFACES AND IRREGULAR SURFACES

Computer simulations were implemented based on the terrain shown in Fig. 7(b). The optimization was carried out in four regions depending on change of the tilt angle, and each region is arranged in Table 4. For the design parameters of the RCGA, the crossover probability, mutation probability, and population size were set to 0.8, 0.3, and 20, respectively. For Regions I, II, III, and IV, the generations were set to 100, 50, 20, and 20, respectively. By the fitness function used in the previous subsection, the performance and stability of the robot locomotion was evaluated. w_1, w_2, w_3, w_4, and w_5 were set to 1, 1, 1, 3, and 0.1, respectively.

Under the similar environmental conditions and specifications of the robot, computer simulations and hardware experiments were performed to verify the performance of admittance control with the IM and the optimized PTS. Because the HUNTER was designed for walking having three contact points (a triangular support polygon) between its feet and the ground, the torque and strength exerted by each of its joints–such as the sunk key and shaft–is insufficient for the robot to climb slanted surfaces in comparison with StarlETH having a similar size. [2].

Thus, an additional scheme is required for HUNTER to climb the uphill trails. In the postural transition region, if the COG projection point moved towards the rear legs, HUNTER lost its balance rapidly owing to the lack of torque and deformations of several mechanical elements. To prevent this problem, a part of the optimized PTS was performed before the initial trot cycle, both in the computer simulations and hardware experiments. Despite unsatisfactory condition occurred by this additional scheme that the COG projection point is shifted towards the front legs on the horizontal and the slanted surfaces, in particular on the horizontal surface, this scheme can lower the joint torque by reducing the movement generated by the PTS. Thus, the robot performed a part of the PTS, which stretched its front legs and rear legs backward by −0.11 m and −0.05 m. For the foot trajectory, the stride, maximum foot height, and single-step period were 0.080, 0.100 m, and 1 s, respectively. The total simulation time was 48.25 s. In this work, ε_i and σ_i are set to 0 and 18, respectively. B_i is the critical damping coefficient that decreases most rapidly in the case of overshoot.

To verify the performance of admittance control with the IM and the optimized PTS, the computer simulations are implemented and compared by the following cases.

- Case I (with IM): Applying admittance control with the IM and the optimized PTS (main scheme)
- Case II (without IM): Applying admittance control without the IM and the optimized PTS
- Case III (without AC): Applying only the optimized PTS
- Case IV (without PTS): Applying only admittance control with the IM

The lower and upper boundaries of the design variables α^π and ν^π for $\pi = r, p$ are

$$0 \le \alpha^\pi \le 7,$$
$$0 \le \nu^\pi \le 0.03.$$

The lower and upper boundaries of the reference stiffness K_0, the variation value of the stiffness K_v^π for $\pi = r, p$, and the gain ζ are

$$3000 \le K_0 \le 5000,$$
$$0 \le K_v^\pi \le 200,$$
$$0 < \zeta \le 1.$$

The lower and upper boundaries of the design variables β^r and β^p are

$$0 \le \beta^r \le 0.15,$$
$$0 \le \beta^p \le 0.06.$$

Tables 5 and 6 present the optimized simulation results. The resultant values of K_0 and ζ were the optimized ones for the simulation that the robot trotted on the horizontal surface. In Regions III and IV, β^π for $\pi = r, p$ had smaller values other than ones of Regions I and II. It means that the robot controlled its body swaying based on more narrow ranges

TABLE 5. Optimization results of individuals (1).

Region	Best score	Design variable											
		α_1^r	α_2^r	α_3^r	α_4^r	α_5^r	α_6^r	α_1^p	α_2^p	α_3^p	α_4^p	α_5^p	α_6^p
I	393.6	1.775	2.017	3.945	4.511	5.117	6.879	1.823	2.031	2.523	4.568	5.827	6.659
II	386.9	1.930	2.781	3.528	4.097	5.768	5.800	0.210	1.207	2.608	3.422	4.982	5.506
III	291.3	1.654	1.666	3.323	4.151	4.228	4.768	1.931	2.016	3.012	3.598	5.251	5.334
IV	291.3	1.793	2.247	4.000	4.512	5.626	5.831	1.095	1.945	3.474	3.885	4.291	6.365

TABLE 6. Optimization results of individuals (2).

Region	Design variable								
	ν^r	ν^p	K_0	K_v^r	K_v^p	$\zeta_f^\dagger$	$\zeta_h^\dagger$	β^r	β^p
I	0.001	0.020	3830.0	193.1	190.7	0.189	0.381	0.153	0.059
II	0.019	0.006	3830.0	162.0	187.8	0.189	0.381	0.151	0.055
III	0.027	0.005	3830.0	11.7	4.5	0.189	0.381	0.064	0.051
IV	0.027	0.006	3830.0	43.7	20.3	0.189	0.381	0.076	0.041

† The subscripts 'f' and 'h' denote the front leg and rear leg, respectively.

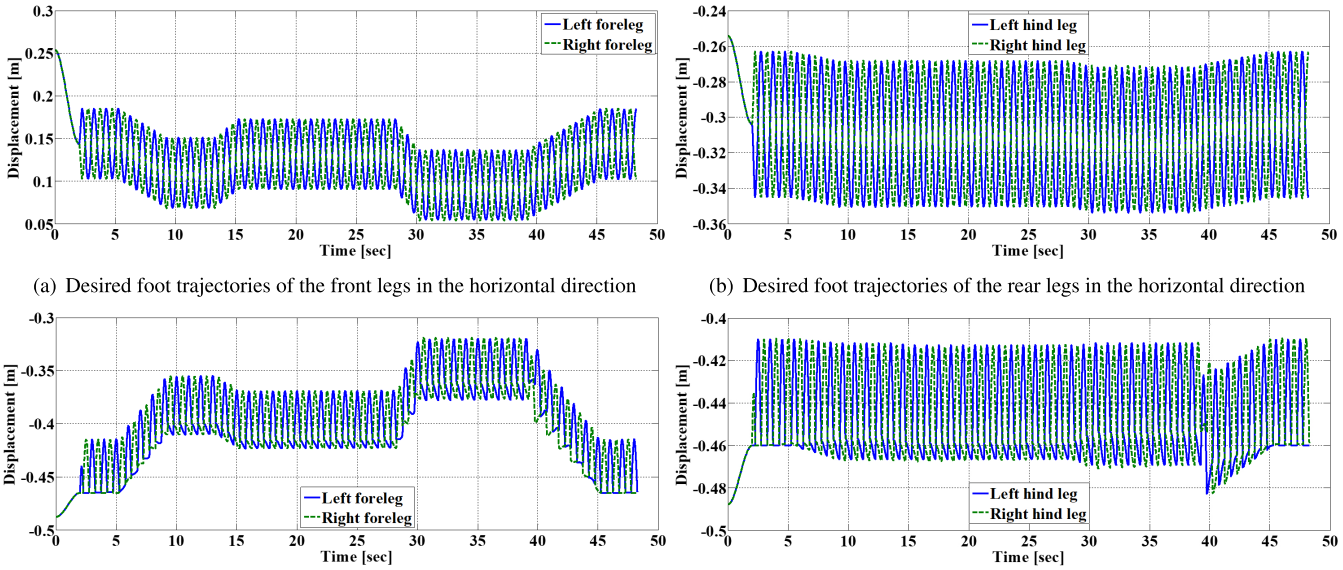

(a) Desired foot trajectories of the front legs in the horizontal direction

(b) Desired foot trajectories of the rear legs in the horizontal direction

(c) Desired foot trajectories of the front legs in the vertical direction

(d) Desired foot trajectories of the rear legs in the vertical direction

FIGURE 9. Simulation results (1): Desired foot trajectories in the computer simulation.

generated by CT^r and CT^p for regions with larger disturbance (Regions III and IV) so that it could rapidly respond to the variation of the swaying.

The optimized PTS is applied to the center point of the desired foot path, as can be seen in Fig. 9, whose movement values present in Table 3. The PTS were mainly performed by the movements of the front legs in the horizontal and vertical directions, which are shown in Fig. 9.

Fig. 10 represents foot trajectories measured by a position sensor. The measured foot trajectories in the horizontal direction, as can be seen in Figs. 10(a), and 10(b), included information, such as the tracking error caused by the GRF and the optimized values for the postural transition. In addition, for the measured foot trajectories in the vertical direction, as can be seen in Figs. 10(c), and 10(d), information of the offset position δ_z generated by admittance control with the IM was added when compared with measured ones in the horizontal direction.

The forward displacements of the robot body for each case, which is shown in Fig. 11. When Case I (with IM) was applied to control the robot posture based on the ranges generated by CT^r and CT^p, the robot exhibited significantly improved forward movement. Case III (without AC) and Case IV (without PTS), the robot did not climb the slanted surface. Moreover, it tipped over after 9.8 s for Case III and 16.4 s for Case IV. The robot controlled by Case II (without IM) could hardly

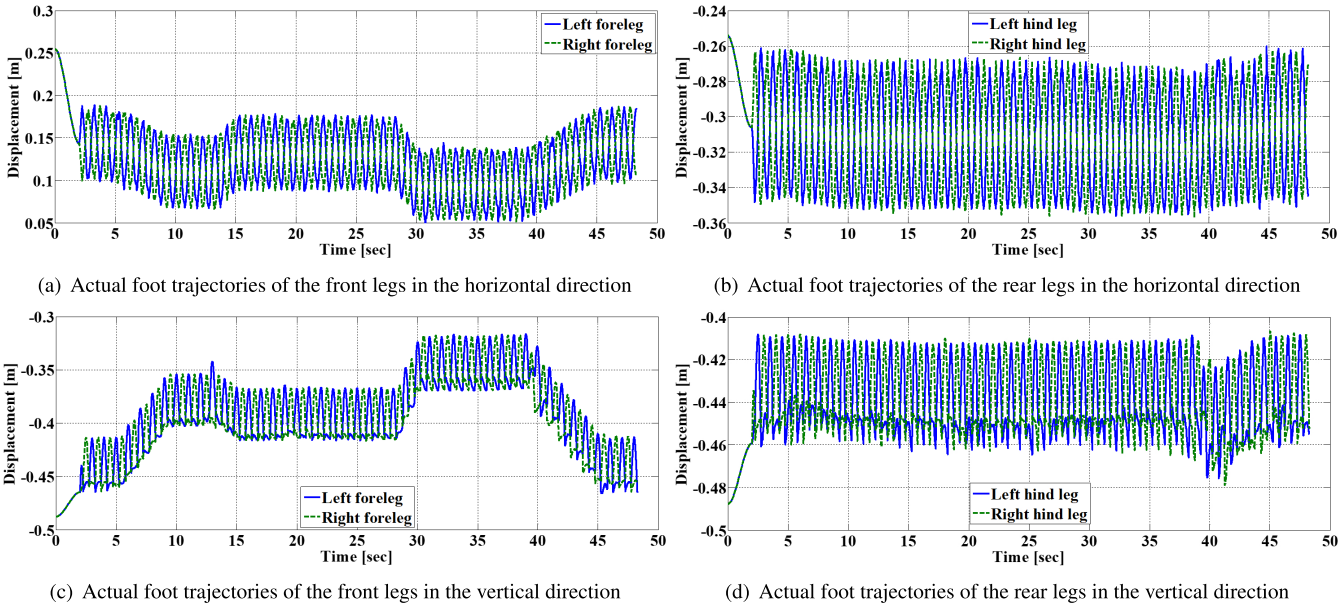

(a) Actual foot trajectories of the front legs in the horizontal direction

(b) Actual foot trajectories of the rear legs in the horizontal direction

(c) Actual foot trajectories of the front legs in the vertical direction

(d) Actual foot trajectories of the rear legs in the vertical direction

FIGURE 10. Simulation results (2): Actual foot trajectories in the computer simulation.

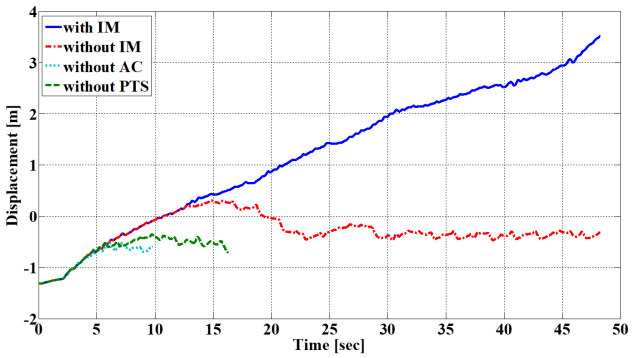

FIGURE 11. Simulation results (3): Forward displacement of the robot body.

move on the slanted surface because of its low movement performance.

Fig. 12 shows the Euler angles of the robot body in comparison with the other cases and Case I (with IM). The ranges generated by CT^r and CT^p were changed depending on the posture transition region, which were reduced by P^r and P^p. In addition, the ranges were moved by the cubic polynomial $\mathbf{f}_{\psi_t}$, as can be seen in Fig. 12(b). For Case I, the figure shows that the roll and pitch angles were not perfectly kept within the ranges generated by CT^r and CT^p, and the range generated by CT^p got narrow greatly by P^p between 15 and 25 s. In addition, for Case I, the roll and pitch angles were maintained at the postural transition region within the ranges generated by CT^r and CT^p to a higher degree when compared with the other cases, which are shown in Fig. 12. However, the pitch increased beyond the range generated by CT^p after 40 s.

For Case I (with IM), the stiffness values changed depending on the roll and pitch angles, as can be seen in Fig. 13, in the result, the angles did not deviate significantly from ranges generated by CT^r and CT^p, as can be seen in Fig. 12. In the other cases, the roll and pitch angles deviated considerably from the ranges. The changes of the stiffness values occurred every quarter-second. It means that N_z was set to four (in the foot landing, foot lift-off, and the moment of the maximum height of the flight phase). The stiffnesses of the legs had similar patterns between 12 and 22 s, as can be seen in Figs. 13(a) and 13(b) (or Figs. 13(c) and 13(d)). It means that the stiffnesses of the left legs or the right legs were mainly regulated by admittance control with the IM based on the roll beyond the range generated by CT^r and η^r.

D. HARDWARE EXPERIMENTS

HUNTER, shown in Fig. 14, is equipped with sensors (IMU and FSR), motor controllers, and motors. In addition, it has passive joints composed of torsional springs and foamed polyurethane pads. The torsional springs with stiffness of approximately 300 Nm/rad and the foamed polyurethane pad with a loss factor of 0.25 are used to decrease the GRF. The specifications of HUNTER match those of the simulation model introduced in Table 1. The motor (Maxson' RE 30) has a nominal output torque of 85.6 mNm and a gearing reduction ratio of 1/102. Thus, the torque produced in each joint is approximately 8.7 Nm. The torque is not sufficient for the robot to climb the uphill trail when compared with other quadruped robots of similar size [2]. Moreover, the mechanical elements of the joints did not have sufficient strength to perform the task. Thus, unlike the computer simulations handled in the previous subsection, the experiment was performed only on flat surfaces with an inclination angle of 10 degrees. In addition, as in the computer simulations, the robot performed a part of the postural transition before

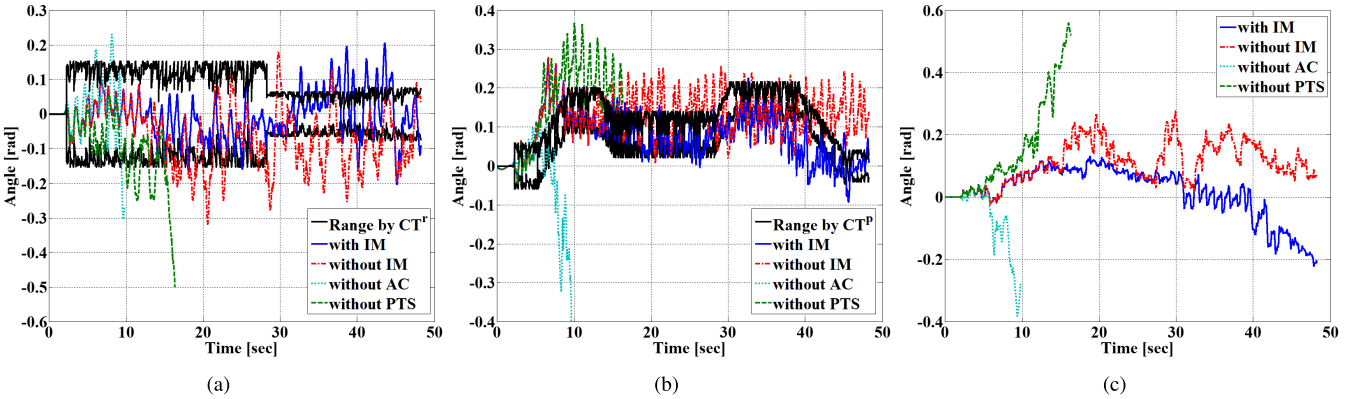

FIGURE 12. Simulation results (4): (a) Roll angles of the robot body, (b) Pitch angles of the robot body, (c) Yaw angles of the robot body.

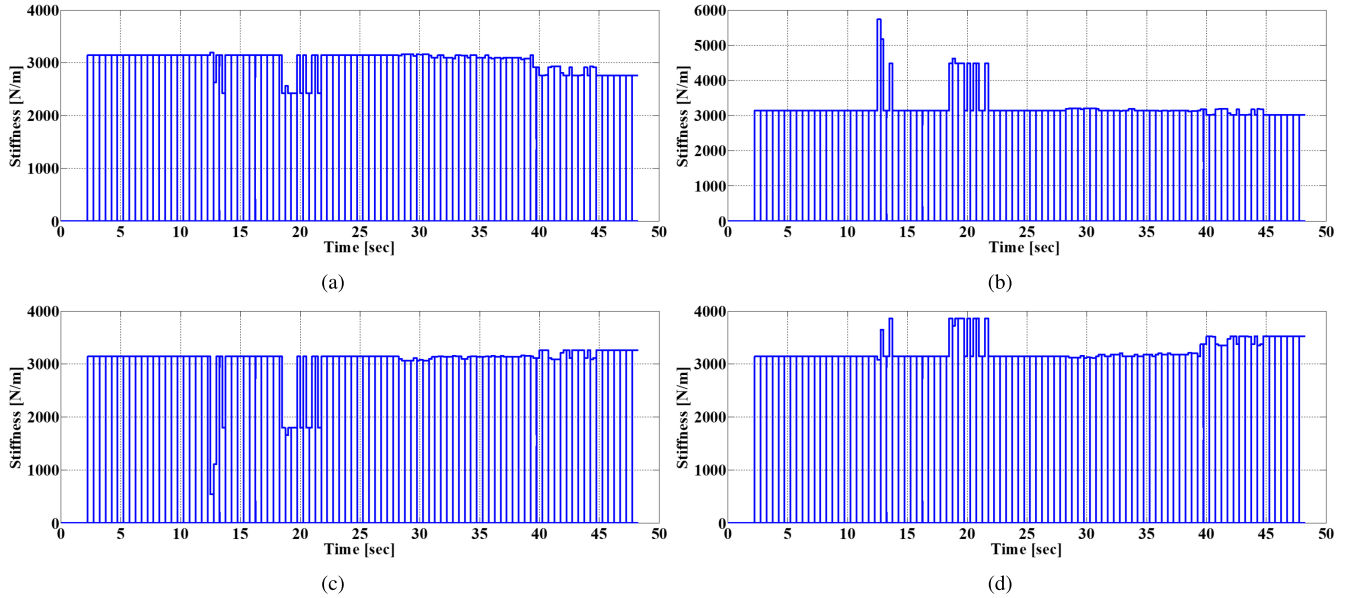

FIGURE 13. Simulation results (5): (a) Stiffness of the left front leg, (b) Stiffness of the right front leg, (c) Stiffness of the left rear leg, (d) Stiffness of the right rear leg.

the initial trot cycle, which stretched its front legs and rear legs backward by −0.11 m and −0.05 m.

Because it is impossible to repeat many hardware experiments under the same conditions, the parameters were tuned not by the optimization, but by trial and error based on the results of computer simulations. The parameters are summarized in Table 7. This table shows that different parameters were used in the computer simulations and the hardware experiment. This was caused by modeling errors, such as gear backlash, joint clearance, and ground condition between the simulation model and the hardware model, which also affected the setting of the ranges generated by CT^r and CT^p. The remaining parameters (not in Table 7) were applied in the same values as those of the simulation. For the foot trajectory, the stride, maximum foot height, single step period, ε_i, and σ_i were equal to those of the simulation. The total number of transition steps N was set to 4 and the total time of the trotting was 7.75 s from 19.75 s to 27.5 s. As in the computer simulations, the hardware experiments are compared with four cases.

Fig. 15(a) shows snapshots of HUNTER trotting on the horizontal and the slanted surfaces by using the proposed schemes–the PTS and admittance control with the IM. The forward displacement was significantly increased by Case I (with IM). Fig. 15(b) shows a snapshot of HUNTER immediately after the locomotion for Case II (without IM). The robot had a short forward displacement when compared with Case I. Figs. 15(c) and 15(d) also present snapshots of HUNTER immediately after the locomotion for Case III (without AC) and Case IV (without PTS). The motion of the right front leg stopped because of the preset limits of the motor controller for tracking error of a position and a velocity, as can be seen in Fig. 15(c). In Fig. 15(d), the robot did not experience leg stops, unlike the experiment of Fig. 15(c).

TABLE 7. Parameters set.

Symbol	Value	Unit	Symbol	Value	Unit	Symbol	Value	Unit
K_0	1,500	Nm^{-1}	η_1^{π}	0.018	rad	α_1^{π}	1	-
K_v^r	50	Nm^{-1}	η_2^{π}	0.035	rad	α_2^{π}	2	-
K_v^p	50	Nm^{-1}	η_3^{π}	0.053	rad	α_3^{π}	3	-
β^r	0.087	rad	η_4^{π}	0.070	rad	α_4^{π}	4	-
β^p	0.051	rad	η_5^{π}	0.088	rad	α_5^{π}	5	-
-	-	-	η_6^{π}	0.110	rad	α_6^{π}	6	-

$\odot\ \pi = r, p$

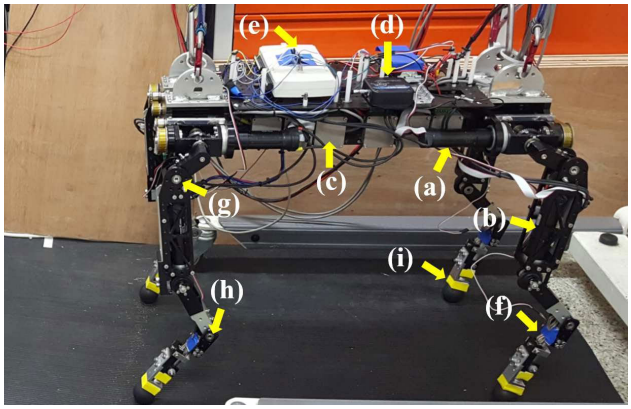

FIGURE 14. HUNTER:(a) and (b) Motors (Maxson RE 30), (c) Motor drive (Elmo whistle), (d) IMU (3DM-GX1), (e) DAQ (NI DAQmx), (f) Force sensor (FSR), (g) and (h) Passive joints (torsional spring), (i) Foamed polyurethane.

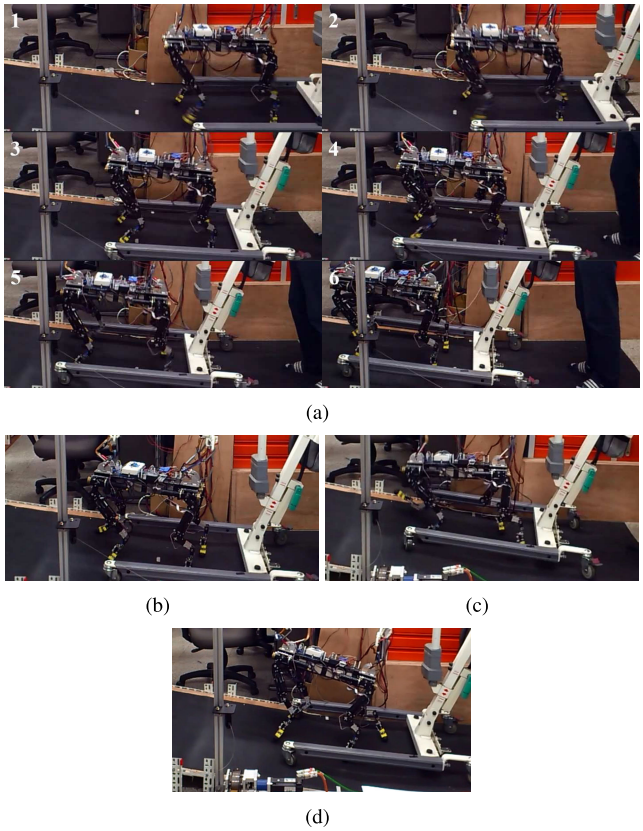

FIGURE 15. Experimental results (1): Snapshots of HUNTER trotting on the horizontal and slanted surfaces: (a) Case I (Applying admittance control with the IM and the optimized PTS), (b) Case II (Applying admittance control without the IM and the optimized PTS), (c) Case III (Applying only the optimized PTS), (d) Case IV (Applying only admittance control with the IM).

However, the robot did rarely trot on the slanted surface because the COG shifted to the rear legs.

The optimized PTS was applied to the desired foot trajectories from 22.5 to 26.5 s, which are shown in Fig. 16. The movement values of the PTS are summarized in Table 3.

Figs. 17(a) and 17(b) show the measured foot trajectories in the horizontal direction. The measured foot trajectories were found by computing forward kinematics of the position values of the motors sensed by the position sensors. The measured foot trajectories of the front legs in the horizontal direction were transformed a lot when compared with the desired ones, as can be seen in Figs. 17(a) and 17(b). It is because admittance control in the horizontal direction is not applied to the foot trajectories owing to the limits of the FSR. In addition, the figures include information, such as the movement values of the postural transition and tracking error. Figs. 17(c) and 17(d) show the measured foot trajectories in the vertical direction. The figures have additional information about the offset position δ_z when compared with the measured ones in the horizontal direction.

Fig. 18 shows the oscillation ranges of the swaying in comparison with the other cases and the ranges generated by CT^r and CT^p for Case I (with IM). In addition, the ranges were reduced by P^r and P^p. For Case I, the roll and pitch angles were kept within the ranges more than the other cases, as can be seen in Figs. 18(a) and 18(b). The range generated by CT^p was moved by $\mathbf{f}_{\psi_\mathbf{t}}$, which is shown in Fig. 18(b). The instrument error at the yaw angle caused by the influence of the magnetometer was calibrated after 20 s, as can be seen in Fig. 18(c).

For Case I (with IM), the stiffness values changed depending on the sizes of the roll and pitch angles beyond the ranges generated by CT^r and CT^p, which are shown in Fig. 19. It means that the algorithm of the IM in Fig. 6 was performed based on the ranges generated by CT^r, CT^p, η^r, and η^p. In addition, the changes occurred every a half-second. It means that N_z was set to two (in the foot landing and foot lift-off). The stiffness values of the right legs were generally

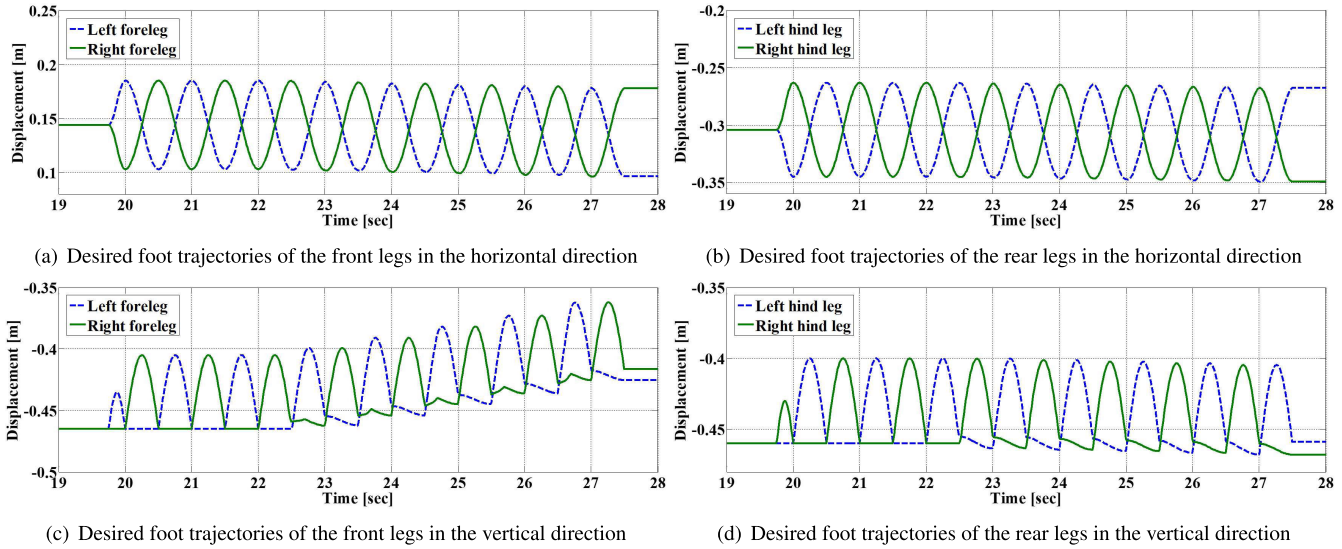

(a) Desired foot trajectories of the front legs in the horizontal direction

(b) Desired foot trajectories of the rear legs in the horizontal direction

(c) Desired foot trajectories of the front legs in the vertical direction

(d) Desired foot trajectories of the rear legs in the vertical direction

FIGURE 16. Experimental results (2): Desired foot trajectories during the experiment.

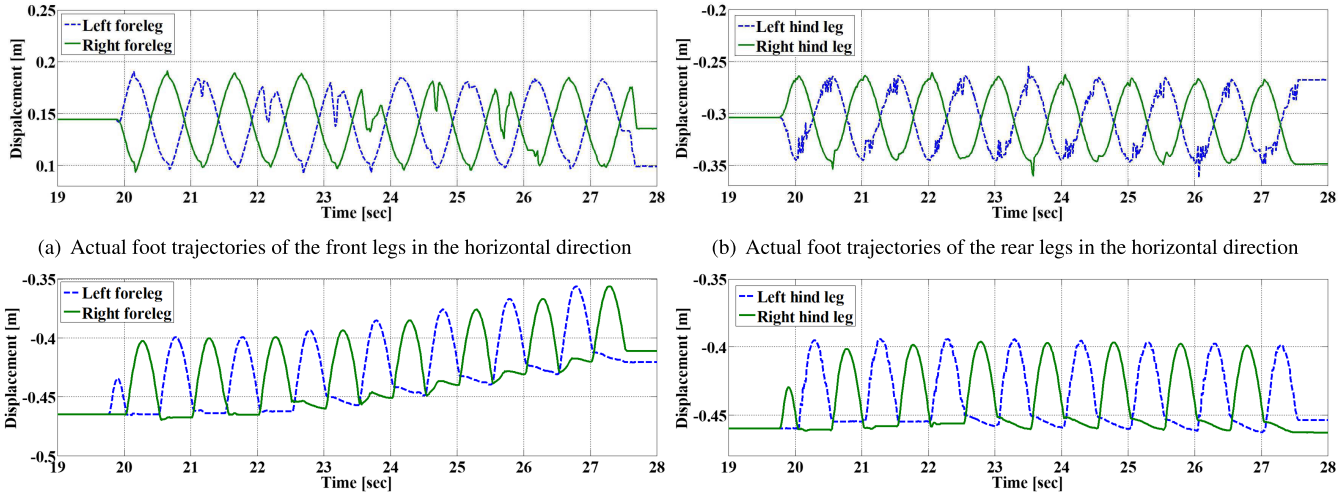

(a) Actual foot trajectories of the front legs in the horizontal direction

(b) Actual foot trajectories of the rear legs in the horizontal direction

(c) Actual foot trajectories of the front legs in the vertical direction

(d) Actual foot trajectories of the rear legs in the vertical direction

FIGURE 17. Experimental results (3): Actual foot trajectories during the experiment.

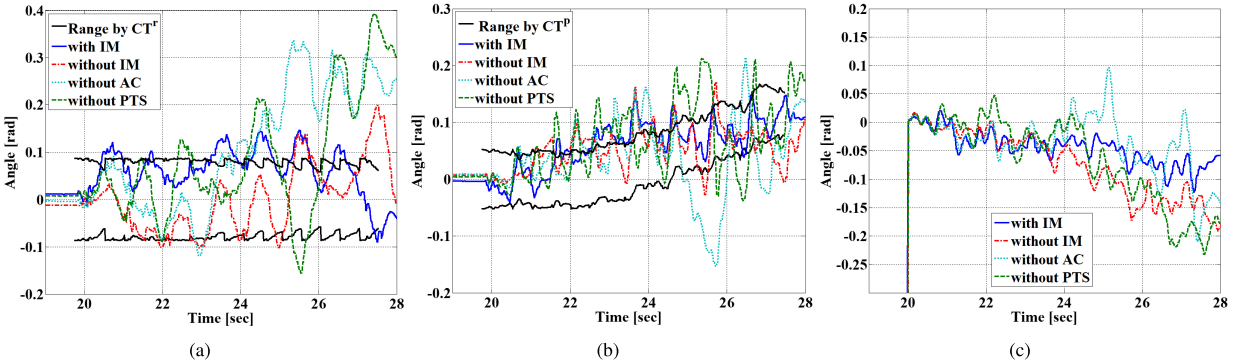

(a) (b) (c)

FIGURE 18. Experimental results (4): (a) Roll angles of the robot body, (b) Pitch angles of the robot body, (c) Yaw angles of the robot body.

larger than those of the left legs, verifying that admittance control with the IM operated well considering the roll and pitch angles and the ranges generated by CT^r, CT^p, η^r and η^p.

The stiffness values had similar patterns, as can be seen in Figs. 19(b) and 19(a) (or Figs. 19(d) and 19(c)), which mean that the stiffnesses of the left legs or the right legs were

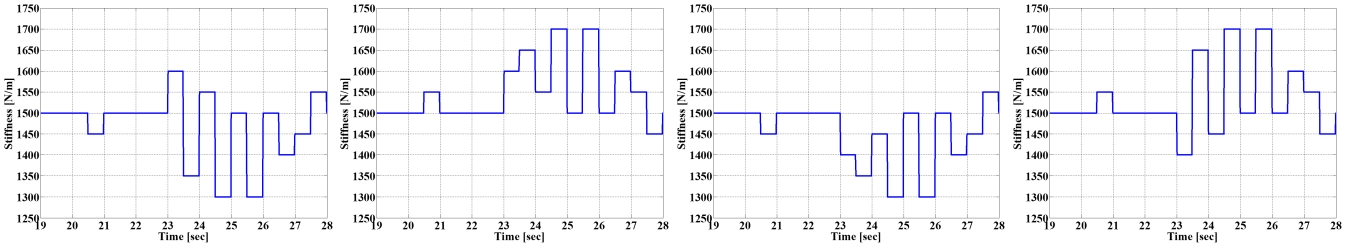

FIGURE 19. Experimental results (5): (a) Stiffness of the left front leg, (b) Stiffness of the right front leg, (c) Stiffness of the left rear leg, (d) Stiffness of the right rear leg.

mainly regulated by admittance control with the IM based on the roll beyond the range generated by CT^r and η^r.

IV. CONCLUSION

A postural transition scheme (PTS) and admittance control with impedance modulation (IM) are proposed to control robot posture on horizontal, slanted, and irregular surfaces including a postural transition section. Control thresholds based on the angular speed of the robot body is proposed as a criterion for controlling the swaying of the robot body by IM. Postural transition is implemented by movement values optimized by a real-coded genetic algorithm (RCGA) depending on the slant angles, and cubic polynomial is used to naturally apply the optimized values. To verify the performance of the proposed schemes, computer simulations and experiments were performed utilizing a 12-DOF quadruped robot called HUNTER. Additional schemes are applied to the simulations and experiments counteract the lack of nominal output torque of the motor and strength reduction of the mechanical elements in each joint. The performance of the proposed scheme was compared with cases when the PTS and admittance control with the IM were not applied to the posture control of the robot. Results of the simulations and experiments verify that the robot trots stably on both horizontal, slanted, and irregular surfaces using the proposed schemes.

REFERENCES

[1] M. Raibert, K. Blankespoor, G. Nelson, and R. Playter, "BigDog, the rough-terrain quadruped robot," *IFAC Proc. Volumes*, vol. 41, no. 2, pp. 10822–10825, 2008.
[2] M. Hutter, M. Gehring, M. Bloesch, C. D. Remy, R. Siegwart, and M. A. Hoepflinger, "StarlETH: A compliant quadrupedal robot for fast, efficient, and versatile locomotion," in *Proc. Int. Conf. Climbing Walking Robots*, 2012, pp. 483–490.
[3] C. Semini, N. G. Tsagarakis, E. Guglielmino, M. Focchi, F. Cannella, and D. G. Caldwell, "Design of HyQ—A hydraulically and electrically actuated quadruped robot," *Proc. Inst. Mech. Engineers, I, J. Syst. Control Eng.*, vol. 225, no. 6, pp. 831–849, 2011.
[4] E. Ackerman. *Spot is Boston Dynamics Nimble New Quadruped Robot*. Accessed: Feb. 10, 2015. [Online]. Available: https://spectrum.ieee.org/automaton/robotics/robotics-hardware/spot-is-boston-dynamics-nimble-new-quadruped-robot
[5] E. Ackerman. *Boston Dynamics' SpotMini is All Electric, Agile, and Has a Capable Face-Arm*. Accessed: Jun. 23, 2016. [Online]. Available: https://spectrum.ieee.org/automaton/robotics/home-robots/boston-dynamics-spotmini
[6] S. Seok, A. Wang, M. Y. M. Chuah, D. J. Hyun, J. Lee, D. M. Otten, J. H. Lang, and S. Kim, "Design principles for energy-efficient legged locomotion and implementation on the MIT cheetah robot," *IEEE/ASME Trans. Mechatronics*, vol. 20, no. 3, pp. 1117–1129, Jun. 2015.
[7] C. Semini, V. Barasuol, J. Goldsmith, M. Frigerio, M. Focchi, Y. Gao, and D. G. Caldwell, "Design of the hydraulically actuated, torque-controlled quadruped robot HyQ2Max," *IEEE/ASME Trans. Mechatronics*, vol. 22, no. 2, pp. 635–646, Apr. 2017.
[8] J. Glower and U. Ozguner, "Control of a quadruped trot," in *Proc. IEEE Int. Conf. Robot. Automat.*, Apr. 1986, pp. 1496–1501.
[9] R. Kurazume, S. Hirose, and K. Yoneda, "Feedforward and feedback dynamic trot gait control for a quadruped walking vehicle," in *Proc. IEEE Int. Conf. Robot. Automat.*, May 2001, pp. 3172–3180.
[10] M. H. Raibert, "Trotting, pacing and bounding by a quadruped robot," *J. Biomech.*, vol. 23, pp. 79–98, Jan. 1990.
[11] R. M. Alexander, *Principles of Animal Locomotion*. Princeton, NJ, USA: Princeton Univ. Press, 2003.
[12] S. Kajita, F. Kanehiro, K. Kaneko, K. Yokoi, and H. Hirukawa, "The 3D linear inverted pendulum mode: A simple modeling for a biped walking pattern generation," in *Proc. IEEE/RSJ Int. Conf. Intell. Robots Syst.*, vol. 1, Oct./Nov. 2001, pp. 239–246.
[13] J. H. Park and K. D. Kim, "Biped robot walking using gravity-compensated inverted pendulum mode and computed torque control," in *Proc. IEEE Int. Conf. Robot. Automat.*, vol. 4, May 1998, pp. 3528–3533.
[14] H. Kimura, Y. Fukuoka, and A. H. Cohen, "Adaptive dynamic walking of a quadruped robot on natural ground based on biological concepts," *Int. J. Robot. Res.*, vol. 26, no. 5, pp. 475–490, May 2007.
[15] L. Righetti and A. J. Ijspeert, "Pattern generators with sensory feedback for the control of quadruped locomotion," in *Proc. IEEE Int. Conf. Robot. Automat.*, May 2008, pp. 819–824.
[16] C. Liu, Q. Chen, and G. Wang, "Adaptive walking control of quadruped robots based on central pattern generator (CPG) and reflex," *J. Control Theory Appl.*, vol. 11, no. 3, pp. 386–392, 2013.
[17] K. Y. Kim, O. Kwon, J. S. Yeon, and J. H. Park, "Elliptic trajectory generation for galloping quadruped robots," in *Proc. IEEE Int. Conf. Robot. Biomimetics*, Dec. 2006, pp. 103–108.
[18] J. H. Lee and J. H. Park, "Control for quadruped robots in trotting on horizontal and slanted surfaces," in *Proc. Asian Control Conf. (ASCC)*, Jun. 2013, pp. 1–6.
[19] L. Sang-Won, O.-H. Kwon, and K.-H. Rim, "Fuzzy controller design for quadruped robot posture control," *Int. J. Digit. Content Technol. Appl.*, vol. 7, no. 12, p. 228, 2013.
[20] X. Chen, K. Watanabe, K. Kiguchi, and K. Izumi, "Optimal force distribution for the legs of a quadruped robot," *Mach. Intell. Robotic Control*, vol. 1, no. 2, pp. 87–93, 1999.
[21] C. Semini, V. Barasuol, T. Boaventura, M. Frigerio, M. Focchi, D. G. Caldwell, and J. Buchli, "Towards versatile legged robots through active impedance control," *Int. J. Robot. Res.*, vol. 34, no. 7, pp. 1003–1020, Jul. 2015.
[22] M. Focchi, A. Del Prete, I. Havoutis, R. Featherstone, D. G. Caldwell, and C. Semini, "High-slope terrain locomotion for torque-controlled quadruped robots," *Auton. Robots*, vol. 41, no. 1, pp. 259–272, 2017.
[23] M. Focchi, G. A. Medrano-Cerda, T. Boaventura, M. Frigerio, C. Semini, J. Buchli, and D. G. Caldwell, "Robot impedance control and passivity analysis with inner torque and velocity feedback loops," *Control Theory Appl.*, vol. 14, no. 2, pp. 97–112, 2016.
[24] D. W. Marhefka, D. E. Orin, J. P. Schmiedeler, and K. J. Waldron, "Intelligent control of quadruped gallops," *IEEE/ASME Trans. Mechatronics*, vol. 8, no. 4, pp. 446–456, Dec. 2003.
[25] J. H. Park, "Impedance control for biped robot locomotion," *IEEE Trans. Robot. Autom.*, vol. 17, no. 6, pp. 870–882, Dec. 2001.
[26] J. Park and J. H. Park, "Impedance control of quadruped robot and its impedance characteristic modulation for trotting on irregular terrain," in *Proc. IEEE/RSJ Int. Conf. Intell. Robots Syst.*, Oct. 2012, pp. 175–180.

[27] A. Lecours, B. Mayer-St-Onge, and C. Gosselin, "Variable admittance control of a four-degree-of-freedom intelligent assist device," in *Proc. ICRA*, May 2012, pp. 3903–3908.
[28] E. Garcia, J. Estremera, and P. G. De Santos, "A comparative study of stability margins for walking machines," *Robotica*, vol. 20, no. 6, pp. 595–606, 2002.
[29] E. G. Papadopoulos and D. A. Rey, "A new measure of tipover stability margin for mobile manipulators," in *Proc. IEEE Int. Conf. Robot. Automat.*, vol. 4, Apr. 1996, pp. 3111–3116.
[30] B. S. Lin and S.-M. Song, "Dynamic modeling, stability, and energy efficiency of a quadrupedal walking machine," *J. Robotic Syst.*, vol. 18, no. 11, pp. 657–670, 2001.
[31] Y. Jia, X. Luo, B. Han, G. Liang, J. Zhao, and Y. Zhao, "Stability criterion for dynamic gaits of quadruped robot," *Appl. Sci.*, vol. 8, no. 12, p. 2381, 2018.
[32] J. H. Park and S. Chung, "Optimal locomotion trajectory for biped robot 'D^2' with knees stretched, heel-contact landings, and toe-off liftoffs," *J. Mech. Sci. Technol.*, vol. 25, no. 1, pp. 3231–3241, 2011.
[33] I. Lim, O. Kwon, and J. H. Park, "Gait optimization of biped robots based on human motion analysis," *Robot. Auton. Syst.*, vol. 62, no. 2, pp. 229–240, 2014.
[34] J. H. Lee and J. H. Park, "Time-dependent genetic algorithm and its application to quadruped's locomotion," *Robot. Auton. Syst.*, vol. 112, pp. 60–71, Feb. 2019.
[35] D. T. Pham and G. Jin, "Genetic algorithm using gradient-like reproduction operator," *Electron. Lett.*, vol. 31, no. 18, pp. 1558–1559, Aug. 1995.
[36] K. Hunt and F. Crossley, "Coefficient of restitution interpreted as damping in vibroimpact," *J. Appl. Mech.*, vol. 42, no. 2, pp. 440–445, Jun. 1975.
[37] *Recurdyn/Solver Theoretical Manual*, FunctionBay, Tokyo, Japan, 2012.

JEONG HOON LEE is currently pursuing the Ph.D. degree with the Department of Mechanical Engineering, Hanyang University, Seoul, South Korea, under the Doctor's Course.

His research interests include quadruped robots, biped robots, industrial robots, robot dynamics, control, learning algorithms, and optimization.

JONG HYEON PARK (M'96) received the B.S. degree in mechanical engineering from Seoul National University, Seoul, South Korea, in 1981, and the S.M. and Ph.D. degrees from the Massachusetts Institute of Technology (MIT), Cambridge, MA, USA, in 1983 and 1991, respectively.

He was a Visiting Researcher with Waseda University, Tokyo, Japan, in 1999, as a part of the Korean Science and Engineering Foundation–Japan Society for the Promotion of Science program, a KOSEF-CNR Visiting Researcher with the Scuola Superiore Sant'Anna, Pisa, Italy, in 2000, and a Visiting Scholar with MIT, from 2002 to 2003, Purdue University, West Lafayette, IN, USA, from 2008 to 2010, and the University of Stuttgart, Germany, in 2019. He was also associated with Brooks Automation Inc., Chelmsford, MA, USA, from 1991 to 1992 and 2001 to 2002. Since 1992, he has been with the School of Mechanical Engineering, Hanyang University, Seoul, where he is currently a Professor. His research interests include biped robots, robot dynamics and control, haptics, and biorobots.

Dr. Park is also a member of The Korean Society of Mechanical Engineers, The Korean Society of Automotive Engineers, the Korean Society of Precision Engineering, and the Institute of Control, Robotics, and Systems. From 2010 to 2017, he has served as a Senior Editor for the *Journal of Mechanical Science and Technology*.